Acoustics Australia
https://doi.org/10.1007/s40857-026-00385-3

ORIGINAL PAPER

Real-Time Cavity Volumetry via Helmholtz Resonance Using Pressure Amplitude: Proof of Concept

Mohammad Amin Barzegar[1] · **Clive E. Davies**[2] · **Miles C. E. Grafton**[3]

Received: 12 November 2025 / Accepted: 9 April 2026

Abstract

Helmholtz resonance provides a well-established acoustic basis for determining volume via the resonance-frequency–volume relationship. However, frequency-tracking methods are typically too slow for dynamic measurements. We present an alternative physical model, the sound-pressure quality-factor (SPQF) model, which estimates volume in real time from cavity sound-pressure amplitude, avoiding frequency hunting. The model follows from the equations governing the driven, underdamped vibration of the port-air mass. The resonator is excited at its empty-cavity natural frequency with a single-tone drive; inserting a sample reduces the steady-state pressure amplitude, from which displaced volume is inferred. We validate the method with liquid and solid samples in 1-, 2-, and 3-L cavities and in a mechanically adjustable chamber under dynamic conditions. The approach achieved millilitre-level accuracy for solids and relative expanded uncertainty $U, k = 2 < 0.1\%$ of cavity capacity in static tests, and it tracked liquid discharge at ~ 15–20 Hz. On the mechanically variable resonator, SPQF tracked piston-driven volume changes for speeds up to 75 mm·s^{-1}, delivering ~ 20 measurements in 1.5 s.

✉ Mohammad Amin Barzegar
Amin.Barzegar@aut.ac.nz

Clive E. Davies
c.davies@massey.ac.nz

Miles C. E. Grafton
m.grafton@massey.ac.nz

[1] AUT AI Research Centre, School of Engineering, Computer and Mathematical Sciences, Auckland University of Technology, 31 Symonds Street, Auckland CBD, Auckland 1010, New Zealand

[2] School of Food Technology and Natural Sciences, Massey University, Private Bag 11 222, Palmerston North 4442, New Zealand

[3] Environmental Sciences, School of Agriculture & Environment, Massey University, Private Bag 11 222, Palmerston North 4442, New Zealand

Published online: 29 May 2026

Graphical Abstract

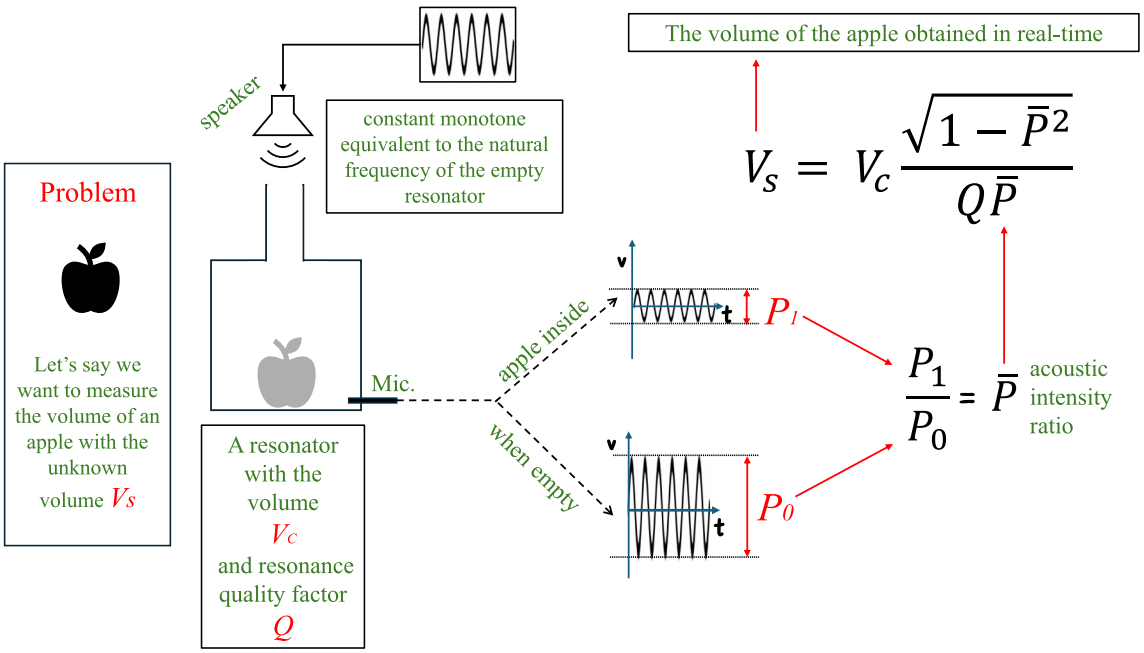

Keywords Helmholtz resonance · Cavity volumetry · Sound pressure quality factor (SPQF) · Real-time volume estimation · Acoustic sensing · Resonator pressure amplitude

List of Symbols

a	Internal port radius (m)
$A_d(\omega)$	Steady-state oscillation amplitude (m)
A_0, A_1	Displacement amplitudes (m)
$\bar{A} = (A_1 / A_0)$	Amplitude-ratio factor (–)
c	Speed of sound in air (m s^{-1})
$Ecap$ %	Capacity-normalised error (%)
F	Force term (F_0 / m) (m s^{-2})
F_0	Amplitude of harmonic drive force (N)
f	Resonance frequency of the Helmholtz resonator (Hz)
$f(t)$	Periodic excitation force (N)
FF	Fill factor (–)
$FWHM$	Full width at half maximum (rad s^{-1})
K	Effective stiffness of the cavity air (spring constant) (N m^{-1})
k_0	Wavenumber associated with ω_0 (m^{-1})
l	Effective port length (m)
m	Mass of air in the port (kg)
P_0, P_1	Cavity pressure amplitudes (Pa)
$\bar{P} = (P_1 / P_0)$	Pressure-amplitude ratio (–)
Q	Resonator quality factor (–)
R_M	Total mechanical damping resistance of the port (N s m^{-1})
S	Log-decay slope (s^{-1})
S_p	Cross-sectional area of the port (m^2)
SNR	Signal-to-noise ratio (–)
T	Time (s)
T, T_1, T_2	Ambient temperature(s) used for sound-speed correction (°C)
V_c	Cavity volume (capacity when empty) (m^3)
V_0, V_1	Cavity volume in States 0 and 1, respectively (m^3)
V_s	Volume of the introduced sample (m^3)
$x(t)$	Instantaneous displacement (m)
δP	Incremental pressure rise (Pa)
δV	Incremental change in cavity volume (m^3)
δx	Small penetration into cavity (m)
γ	Ratio of specific heats (–)
Γ	Damping constant (s^{-1})
Z	Damping ratio (–)
ρ	Density of air (kg m^{-3})
ω	Angular frequency (rad s^{-1})
ω_d	Damped frequency (rad s^{-1})
ω_0	Natural angular frequency (empty) (rad s^{-1})
ω_1	Natural angular frequency (with sample) (rad s^{-1})
ω_n	Natural angular frequency (rad s^{-1})

ω_r Driven resonance frequency (rad s^{-1})

1 Introduction

Measuring object volume is challenging—especially when the volume varies in time. Among non-contact approaches, Helmholtz resonance is attractive because the resonance frequency depends on cavity volume; however, frequency-tracking methods are typically too slow for rapidly changing volumes. Outside acoustics, alternatives include hydrostatic level measurement, which is accurate but slow and unsuitable for porous media [7], gas pycnometry [1, 34], and geometric methods using optical, laser, or ultrasonic scanning [2, 3, 5, 28].

Helmholtz-based volumetry exploits the dependence of resonance frequency on cavity volume and has been applied across a range of scales and environments. Nishizu et al. [25] demonstrated automatic, continuous food-volume measurement on a conveyor line using a three-port resonator. Nakano et al. [24], [23] extended the principle to cryogenic liquids under microgravity, measuring liquid volumes in closed resonators, Nakano and Nishizu [22] later applied the technique to liquid-hydrogen level gauging. Chen et al. [10] applied Helmholtz resonance for preliminary watermelon volume estimation. Njane et al. [26] developed an underwater resonator with an open cavity for submerged sample measurement. Li et al. [17], [18] analysed parameters affecting on-orbit propellant gauging via cavity resonance, including the effects of droplets and bubbles, while Crosby et al. [11] demonstrated modal propellant gauging for both settled and unsettled liquids in reduced gravity. Indenbom and Pogossian [13] characterised the resonance behaviour of partially filled Helmholtz resonators analytically, providing frequency and quality-factor predictions as functions of fill level. García et al. [12] developed a non-intrusive tank fill-level sensor that relates exterior acoustic resonance frequency to internal fluid volume without requiring direct access to the tank contents. Webster, [36] and Webster and Davies [37] achieved ± 0.1% capacity-normalised accuracy for static measurements up to 3 L using statistical calibration—but required approximately 40 s of frequency-hunting acquisition. The present authors have investigated Helmholtz-based granular volume determination in hoppers [4]. Beyond resonance-based methods, recent robotics research has explored acoustic sensing for real-time liquid volume estimation: Wilson et al. [38] used audio-visual neural networks to estimate the weight of liquid poured into a container from the pouring sound, and Liang et al. [19] combined audition with haptic feedback to predict liquid height during robotic pouring tasks. These approaches highlight the growing interest in acoustic methods for dynamic volume estimation, though they rely on data-driven models rather than a physics-based resonator relationship. In general, resolving resonance frequency with sufficient precision requires seconds of data through narrow spectral bins or curve fitting, limiting dynamic applications.

A Helmholtz resonator is a cavity with one or more ports; when excited, it resonates at:

$$f = \frac{c}{2\pi}\sqrt{\frac{S_p}{V_c l}} \tag{1}$$

where f is the resonance frequency, c is the speed of sound, S_p is the port cross-sectional area, V_c is the cavity volume, and l is the effective port length. The effective length equals the physical length plus an end correction Δl, because some external air oscillates with the port flow and acts as added mass. Typical values are $0.6a$ for an internal flanged end and $8a/3\pi$ for an external unflanged end, where a is the port radius [9, 14, 30], Blackstock [6].

Equation (1) assumes dimensions small relative to the acoustic wavelength, an incompressible port-air slug, and nearly uniform cavity compression. Extended models address geometric nonlinearities and flow effects [27, 32, 33].

Because f depends on V_c, introducing a liquid or solid changes the resonance and enables volumetry. Prior work has demonstrated this principle, e.g. conveyor-fed samples in a three-port resonator [25], cryogenic propellants in microgravity [22, 24], and static measurements up to 3 L with ± 0.1% capacity-normalised accuracy, but requiring ~ 40 s of frequency-hunting acquisition [36, 37]. In general, resolving frequency with sufficient precision requires seconds of data (narrow bins/curve fits), limiting dynamic applications.

To address the speed limitation, Webster [36]) developed Q-profile shifting (QPS), in which the amplitude drop caused by a sample is used to infer the new resonance frequency from a pre-acquired resonance-peak profile, avoiding a full frequency scan and reducing acquisition to 2–3 s. However, because the inferred frequency is still converted to volume through the Helmholtz equation (Eq. 1), QPS required geometry-dependent empirical correction curves and was limited to fill fractions below approximately 15% of cavity capacity, beyond which the profile-shape assumption underlying the frequency inference degraded.

Here, we propose an acoustics-based approach that enables near-instantaneous volumetry with high accuracy. We derive a model, termed the sound-pressure quality-factor (SPQF), based on the underdamped, forced oscillation of the port-air mass. Sample volume is inferred from the steady-state cavity-pressure amplitude under single-tone excitation at the empty-cavity natural frequency. This approach eliminates the need for frequency hunting and spectral analysis

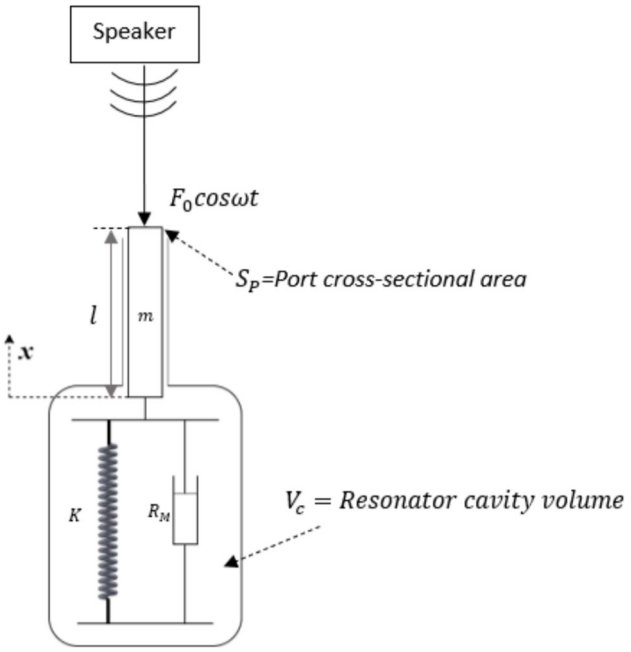

Fig. 1 A Helmholtz resonator analogous to a mass–spring–damper system

by directly inferring volume from sound pressure, enabling real-time measurements.

We validate the method on liquids and solids in 1–3-L resonators and in a mechanically adjustable chamber under static and dynamic conditions. Unlike traditional frequency-tracking Helmholtz volumetry [4, 21, 24, 37], our pressure-based measurement provides effectively instantaneous updates for rapidly changing volumes.

2 Theory

2.1 Mass–Spring–Damper Analogy

To develop the SPQF model, we first recall the mass–spring–damper analogue of a Helmholtz resonator and collect the minimal governing relations that underpin the derivation that follows. A Helmholtz resonator is well-approximated by a lumped mass–spring–damper oscillator (Fig. 1) [6, 20, 31, 35].

The air plug in the port, of mass m, undergoes small in–out displacements x. The compressible cavity air provides a linear restoring force with stiffness K, and acoustic losses are represented by a mechanical resistance R_M (radiation, viscous, and thermal). Radiation resistance depends on port geometry, sound speed, fluid density, and frequency [6, 16]. Viscous and thermal losses scale with frequency and are effectively independent of sound pressure except at very high levels Ingard [14]

The underdamped, forced motion of the port-air mass is.

$$m\frac{d^2x}{dt^2} + R_M\frac{dx}{dt} + Kx = f(t) \tag{2}$$

where $f(t)$ is a periodic drive and t is time. With single-tone excitation from a loudspeaker at angular frequency ω, $f(t) = F_0 cos\omega t$, so $m\frac{d^2x}{dt^2} + R_M\frac{dx}{dt} + Kx = F_0 cos\omega t$.

The natural frequency is $\omega_n = \sqrt{K/m}$. The port-air mass is $m = \rho S_p l$ (air density ρ, port area S_p, effective length l). For small perturbations, the cavity obeys $PV_c^{\gamma} = const$, giving $\delta P/P_0 = -\gamma\,\delta V/V_c$ with $V = S_p\,\delta x$. The resulting restoring force on the plug is $F_m = S_p\,\delta P$; hence, the stiffness is $K = \gamma S_p^2 P_0/V_c$. Using $c^2 = \gamma P_0/\rho$, the natural frequency becomes $\omega_n^2 = c^2 S_p/(lV_c)$. Dividing Eq. 2 by m gives Eq. 3 where $\Gamma = R_m/m$ is the system damping constant and $F = F_0/m$. The steady-state solution is Eq. 4 with amplitude A_d being Eq. 5. At resonance ($\omega = \omega_n$), thus, the amplitude A_0 can be obtained in the form of Eq. 6, which rearranges to the drive term in Eq. 7.

$$\frac{d^2x}{dt^2} + \Gamma\frac{dx}{dt} + \omega_n^2 x = F\cos\omega t \tag{3}$$

$$x(t) = A_d cos(\omega t + \phi) \tag{4}$$

$$A_d(\omega) = \frac{F}{\sqrt{(\omega_n^2 - \omega^2)^2 + \Gamma^2\omega^2}} \tag{5}$$

$$A_d(\omega_0) = \frac{F}{\Gamma\omega_n} = A_0 \tag{6}$$

$$F = A_0\Gamma\omega_n \tag{7}$$

The damping ratio ζ is defined as the ratio of the system's damping to the system's critical damping. Equation 8 is the relationship between the damping constant Γ and damping ratio ζ [15]:

$$\Gamma = 2\zeta\omega_n \tag{8}$$

Consider two operating states (Fig. 2). In both, the port-air mass is driven sinusoidally at ω_0, the natural frequency of the empty resonator (State 0). Introducing a sample of volume V_S changes the parameters from (A_0, P_0, ω_0, V_0, ζ_0) to (A_1, P_1, ω_1, V_1, ζ_1)(State 1). Our goal is to infer V_S from these changes.

Substituting Eqns. (7) and (8) into Eq. 5 for State 1, while maintaining the drive frequency at the natural frequency $\omega = \omega_0$, gives Eq. 9.

$$A_1 = \frac{2A_0\zeta_0\omega_0^2}{\sqrt{\left(\omega_1^2 - \omega_0^2\right)^2 + (2\zeta_1\omega_1\omega_0)^2}} \tag{9}$$

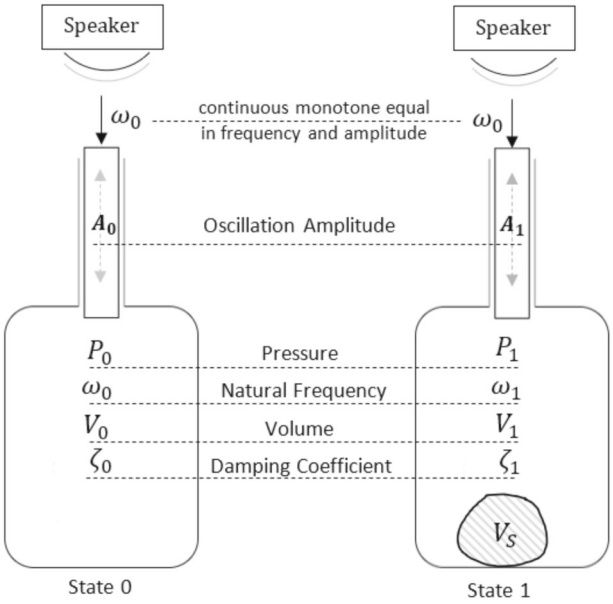

Fig. 2 Two resonator states before and after putting a sample with volume V_s into it

Between States 0 and 1, the oscillation frequency remains constant. As discussed earlier, the total damping of the system R_M depends on the oscillation frequency and port and is independent of sound pressure [6, 14]. Therefore, R_M remains constant between the two states, and likewise $R_M/m = \Gamma$ is constant; thus, from Eq. 8, $\zeta_0\omega_0 = \zeta_1\omega_1$. By implementing this in Eq. 9 and defining $\overline{A} = A_1/A_0$ as the dimensionless oscillation amplitude ratio, Eq. (9) can be written as Eq. (10), which defines the oscillation amplitude ratio factor as a function of the system damping ratio and natural frequency in State 1.

$$\overline{A} = \frac{2\zeta_0\omega_0^2}{\sqrt{\left(\omega_1^2 - \omega_0^2\right)^2 + \left(2\zeta_0\omega_0^2\right)^2}} \tag{10}$$

2.2 Sound Pressure Quality Factor Model

Relating port-air displacement to cavity air pressure via the cavity stiffness in each state which can be represented in the mathematical form: $K_0A_0 = S_pP_0$, $K_1A_1 = S_pP_1$, gives Eq. 11. With m unchanged and $\omega_n^2 = K/m$, we have Eq. 12. Defining the pressure-amplitude ratio in Eq. 13 then leads to Eq. 14. For a resonator with a low damping ratio $\zeta_0 \lesssim 0.05$, the quality factor satisfies the approximation given by Eq. 15. These relations in Eqns. 10, 14, and 15 can be used to link $\bar{P}$ to ω_1/ω_0 and, ultimately, to V_S.

$$\frac{A_1}{A_0} = \frac{P_1}{P_0}\frac{K_0}{K_1} \tag{11}$$

$$\frac{K_1}{K_0} = \frac{\omega_1^2}{\omega_0^2} \tag{12}$$

$$\overline{P} = \frac{P_1}{P_0} \tag{13}$$

$$\overline{A} = \overline{P}\frac{\omega_0^2}{\omega_1^2} \tag{14}$$

$$Q \approx \frac{1}{2\zeta_0} \tag{15}$$

Combining Eqns. 10, 14, 15 gives Eq. 16.

$$\overline{P}\frac{\omega_0^2}{\omega_1^2} = \frac{\frac{1}{Q}\omega_0^2}{\sqrt{\left(\omega_1^2 - \omega_0^2\right)^2 + \left(\frac{1}{Q}\omega_0^2\right)^2}} \tag{16}$$

Equation 16 can be solved for ω_1 to describe the system's natural frequency in State 1 (ω_1) as a function of cavity pressure-amplitude ratio ($\overline{P}$). This operation involves solving a quadratic equation. The solutions of Eq. 16 for ω_1 are:

$$\omega_1 = \begin{cases} (a)\omega_0\sqrt{\dfrac{+\overline{P}\sqrt{\left(1+Q^2-\overline{P}^2Q^2\right)}+\overline{P}^2Q^2}{\overline{P}^2Q^2-1}} \\ (b)-\omega_0\sqrt{\dfrac{+\overline{P}\sqrt{\left(1+Q^2-\overline{P}^2Q^2\right)}+\overline{P}^2Q^2}{\overline{P}^2Q^2-1}} \\ (c)\omega_0\sqrt{\dfrac{-\overline{P}\sqrt{\left(1+Q^2-\overline{P}^2Q^2\right)}+\overline{P}^2Q^2}{\overline{P}^2Q^2-1}} \\ (d)-\omega_0\sqrt{\dfrac{-\overline{P}\sqrt{\left(1+Q^2-\overline{P}^2Q^2\right)}+\overline{P}^2Q^2}{\overline{P}^2Q^2-1}} \end{cases} \tag{17}$$

where *(b)* and *(d)* can be discarded because the resonance frequency cannot be negative.

Because there is an inverse relationship between cavity volume and system resonance frequency $\omega_n^2 = (c^2S_p)/(lV_c)$ and in moving from State 0 to State 1, the cavity volume is decreased by V_s, the system resonance frequency is expected to increase $\left({}^{\omega_1}/_{\omega_0} > 1\right)$, which is satisfied by solution (a).

The natural frequencies in States 0 and 1 are $\omega_0^2 = c^2S_p/(lV_0)$ and $\omega_1^2 = c^2S_p/(lV_1)$, respectively, and subsequently Eq. 18 can be written by division of these natural frequencies for the two states. The sample volume, V_s, can be calculated using Eq. 19 (given that $V_1 = V_c - V_s$). This equation referred to as the "Full" model. For resonance with high Q, which is typical for a single-port Helmholtz resonator without a damper, Eq. 19 can be approximated to Eq. 20, as shown in Fig. (3). For $Q = 10$, there is a deviation of roughly 0.8% between Eq. 19 (shown by "Full" in the legend) and

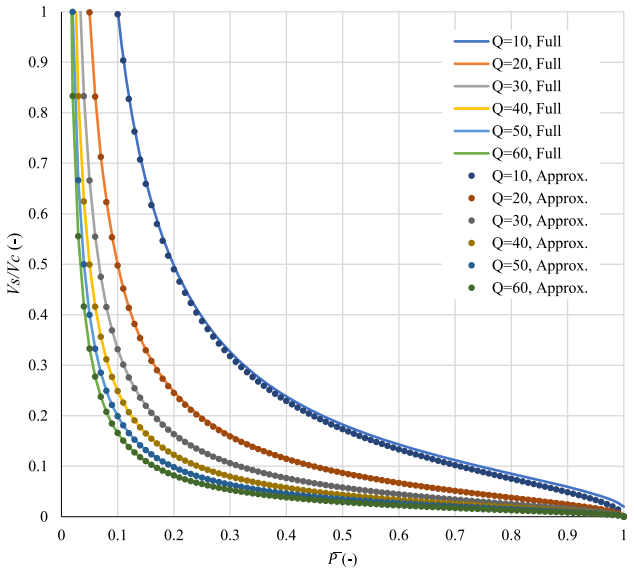

Fig. 3 Numerical comparison of the complete model (Full) vs. its approximated form (Approx)

its approximation in Eq. 20 (shown by "Approx." in the legend). Moving to $Q = 40$ and higher, the deviation between the results obtained using Eqns. 19 and 20 becomes negligible.

The model expressed by Eq. 19 and its approximation at Eq. 20 is referred to Sound Pressure Quality Factor (SPQF) model.

An advantage of the approximation in Eq. 20 is its interpretability in a way that at $\overline{P} = 1$ it predicts $V_s = 0$, and the explicit $1/Q$ scaling makes the dependence of volume on quality factor and pressure ratio transparent.

$$\frac{\omega_1^2}{\omega_0^2} = \frac{V_0}{V_1} \tag{18}$$

$$V_s = V_c \frac{Q\sqrt{1 + \frac{1}{Q^2} - \overline{P}^2} + \overline{P}}{\overline{P}(Q^2 + 1)} \tag{19}$$

$$V_s \cong V_c \frac{\sqrt{1 - \overline{P}^2}}{Q\overline{P}} \tag{20}$$

2.3 Effect of Ambient Temperature

In the development of models for estimating V_S, it was assumed that the drive frequency is equal to the natural frequency of the empty resonator. Variations in temperature affect the speed of sound, which changes the natural frequency of the empty resonator; hence, the drive frequency should change to match the natural frequency accordingly. The drive frequency can be adjusted to match the empty resonator resonance frequency, using the ambient temperature.

Take ω_{0T1} to be the experimentally measured resonance frequency of the empty resonator at the temperature T_1 where the speed of sound is c_{T1}.

When the ambient temperature changes to T_2 and the speed of sound becomes c_{T2}, the resonator's natural frequency ω_{0T2} can be expressed as $\omega_{0T2}^2 = c_{T2}^2 S_p/(lV_c)$, and similarly, for ω_{T1} the expression is $\omega_{0T1}^2 = c_{T1}^2 S_p/(lV_c)$. The division of these states gives:

$$\frac{\omega_{0T2}}{c_{T2}} = \frac{\omega_{0T1}}{c_{T1}} \tag{21}$$

which is equivalent to k_0, the wavenumber is associated with the empty resonator's natural frequency and remains constant with temperature variation. Obtaining k_0 is crucial for the experimental measurements.

The sound speed in air at a specific temperature can be readily estimated using the equation $c = 331.45\sqrt{1 + T/273}$ [8]. With this sound speed estimation, Eq. 22 can be used to adjust drive frequency based on the ambient temperature change. As long as the drive frequency at the time of sample volume measurement (ω_{0T2}) matches the natural frequency of the empty resonator, the sample volume in the SPQF model mathematically remains unaffected by changes in ambient temperature and resonance frequency.

$$\omega_{0T2} = \frac{\sqrt{1 + \frac{T2}{273}}}{\sqrt{1 + \frac{T1}{273}}}\omega_{0T1} \tag{22}$$

2.4 Natural Frequency

In State 0, where the resonator is empty, the maximum resonance amplitude occurs when the derivative of $A_d(\omega)$ in Eq. 5 goes to zero. This obtains Eq. 23, which correlates the driven underdamped resonance frequency ω_r to the natural frequency of the system ω_0. Combining Eqs. 8 and 23 gives Eq. 24.

$$\omega_r = \sqrt{\omega_0^2 - \Gamma^2/2} \tag{23}$$

$$\omega_0 = \frac{\omega_r}{\sqrt{1 - 2\zeta_0^2}} \tag{24}$$

As seen in Eq. 23, an underdamped resonator exhibits a small offset between the natural frequency and the driven resonance frequency. In practice, we locate the State-0-driven resonance ω_r by exciting the system with white noise or a continuous chirp and identifying the spectral peak. With the damping ratio ζ known, Eq. 24 then gives the excitation frequency ω_0. For heavily underdamped systems ($\zeta \ll 0.05$),

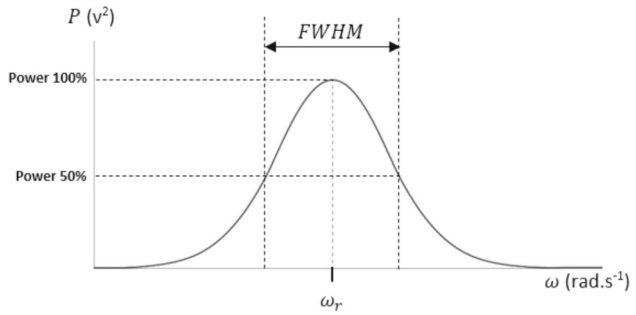

Fig. 4 Quality factor and resonance frequency determined from power spectral analysis. (Although the Lorentzian peak shape is standard, the figure is included to explicitly illustrate the practical extraction of Q via FWHM and ω_r)

$\sqrt{1-2\zeta_0^2} \approx 1$, so $\omega_0 \approx \omega_r$. In the experiments below we use Eq. 24; however, when Q is high the approximation $\omega_0 \approx \omega_r$ is effectively equivalent. Although ω_r is obtained empirically, we still apply the damping correction via ζ using Eq. 24 to obtain ω_0 as the input to the SPQF model.

2.5 Quality Factor

2.5.1 Driven Resonance

The Resonator Quality Factor can be estimated using spectral analysis, as shown in Fig. 4. When a Helmholtz resonator is continuously excited using white noise or a chirp, the pressure is converted to a voltage signal and then transformed to the frequency domain using power spectral density analysis, resulting in a graph like what is shown Fig. 4, a graph of power P vs frequency ω. The resonance frequency ω_r is the frequency at which the power reaches its maximum value. The estimated resonance quality factor can be calculated, using Eq. 25, from the shape of the curve obtained, which can be considered to be Lorentzian [15, 35].

$$Q \approx \frac{\omega_r}{FWHM} \tag{25}$$

Quality factor can also be determined using a reference sample. When a sample of material with a known volume V_A is in the resonator, quality factor can be determined through the rearrangement of Eq. 20 to the form of Eq. 26.

$$Q = V_c \frac{\sqrt{1-\overline{P}^2}}{V_A \overline{P}} \tag{26}$$

2.5.2 Undriven Resonance

When exciting a Helmholtz resonator with an impulse (undriven oscillation), the resonator response decays at a rate proportional to ζ (damping ratio). In the general oscillation model shown in Eq. 2, if the drive force $f(t)$ vanishes, the solution for the displacement of the port's air mass can be written in the form of Eq. 27, where $e^{-\zeta\omega_0}$ is the logarithmic decay rate of the amplitude. The slope of this line (S in Eq. 28) is the decay rate in Eq. 27 ($ln(x) = -\zeta\omega_0 t$). Resonance frequency (ω_r) in undriven response ω_d is slightly lower than natural frequency, as shown in Eq. 29 [29]. The displacement of amplitude x in a Helmholtz resonator is presented, as the ordinate, in the schematic diagram in Fig. 5A. Fluctuations in $x(t)$ result in pressure fluctuations inside the cavity with the same decay rate. A line is obtained by locating the pressure maxima, taking logarithms, and plotting against time (Fig. 5B). Given that $Q \approx 1/2\zeta_0$, Eq. 30 can be derived to estimate quality factor empirically from resonator impulse response. ω_r can be obtained by counting the number of oscillations per second as the oscillation amplitude decays, as shown in the schematic Fig. 5A.

$$x(t) = Ae^{-\zeta\omega_0 t} cos(\omega_r t + \phi) \tag{27}$$

$$-\zeta\omega_0 t = St \tag{28}$$

$$\omega_d = \omega_0\sqrt{1-\zeta^2} \tag{29}$$

$$Q = \frac{1}{2}\sqrt{\frac{\omega_r^2 + S^2}{S^2}} \tag{30}$$

3 Materials

3.1 Sample Volume Measurement Apparatus

The experimental apparatus (Fig. 6) comprised a modular acrylic Helmholtz resonator with interchangeable cavities and ports, a pressure-type microphone, a commercial speaker driver, a temperature sensor, and signal conditioning electronics. The resonator consisted of a cylindrical cavity (ID 140 mm; three available heights: 60, 123, 195 mm) clamped between 10-mm acrylic top and bottom plates using bolts and O-ring seals. The top plate had a central 50-mm port opening and a lateral bore located 50 mm off-centre for microphone placement. Ports were constructed from aluminium tubing (ID 44 mm; lengths: 51 mm and 170 mm). The bottom plate was interchangeable, with one variant drilled to allow liquid discharge during dynamic tests.

Temperature was monitored using an LM35 precision sensor (Texas Instruments; ± 0.5 °C manufacturer specification) verified against a mercury reference thermometer (Brannan; 0.1 °C resolution) across the operating range (15–25 °C). Conservative ± 2 °C uncertainty used in analysis accounts

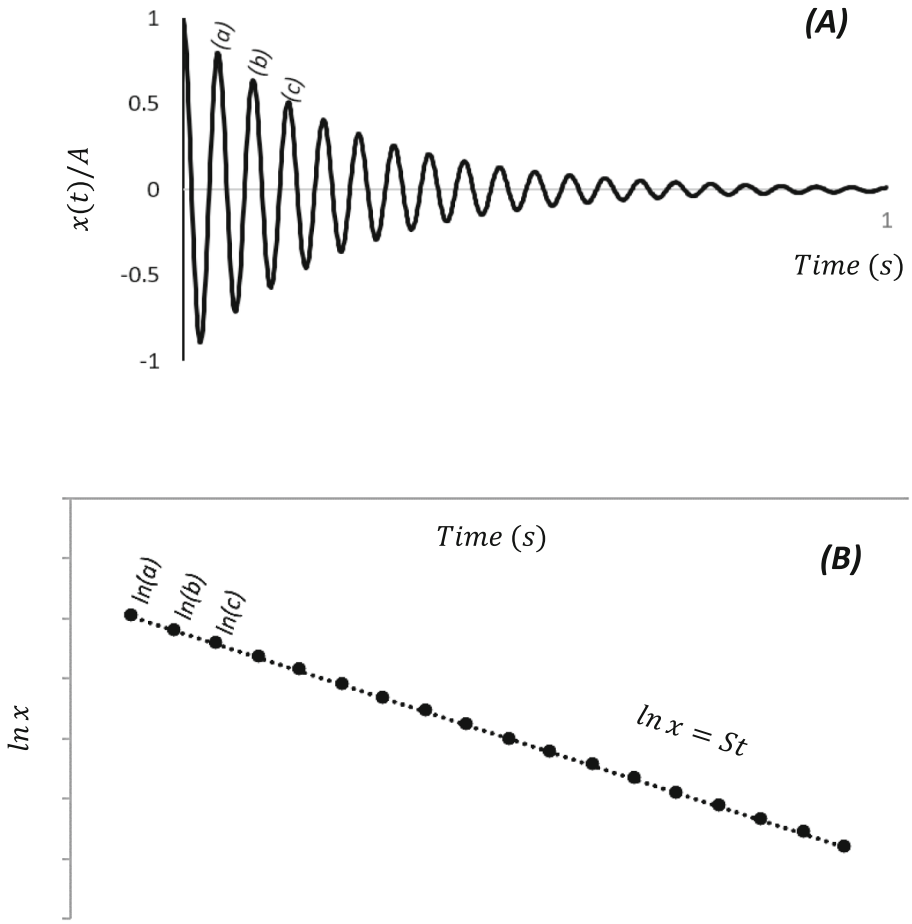

Fig. 5 **A** Schematic signal decay in an underdamped, undriven resonance of a Helmholtz resonator. **B** Logarithmic amplitude decay line

for sensor accuracy, spatial gradients, and temporal variations.

Cavity pressure was measured using a precision pressure transducer (PCB Piezotronics Model 103A; sensitivity 1500 mV/psi; linearity ± 2% full scale; frequency response 0.05 Hz to 13 kHz) coupled to a low-noise signal conditioner (PCB Model 482A18; 8-channel ICP power supply; signal-to-noise ratio > 90 dB at × 10 gain). All resonators operated in the frequency range 85–242 Hz, well within the transducer's flat response region. Because the SPQF method uses pressure ratios ($\overline{P} = P_1/P_0$) measured sequentially with the same sensor at fixed frequency, absolute sensitivity specifications cancel mathematically. Only linearity (± 1% over the operating range 3–83 Pa) and short-term drift (0.054%/ °C) contribute to systematic uncertainty. The pressure transducer was positioned 40–50 mm from the port opening to minimise interference with port airflow while ensuring adequate signal strength. At the operating frequencies (85–242 Hz, corresponding to acoustic wavelengths 1.4–4 m), the cavity behaves as a lumped acoustic system with a nearly uniform pressure distribution, making precise transducer placement non-critical. Because measurements use pressure ratios ($\bar{P} = P_1/P_0$) acquired at the same location for both states, positional variations in absolute pressure cancel.

Acoustic excitation was delivered using a 100-mm Pioneer TS-G1020F speaker driver mounted 200 mm above the resonator in a polyethene cylinder lined with glass wool. Ambient temperature was recorded using an LM35 sensor placed near the port.

The system was controlled using a Data Acquisition (DAQ) card (USB-6211, National Instruments, USA) with the sampling rate: 44,100 Hz. The excitation signal (sinusoidal, fixed frequency) was generated and applied through the DAQ output channel, while the microphone response was recorded via the input channel. Both signals were acquired simultaneously and synchronously using the same sampling clock. Each measurement used an averaging window of 20–50 ms, equivalent to 10–20 pressure cycles.

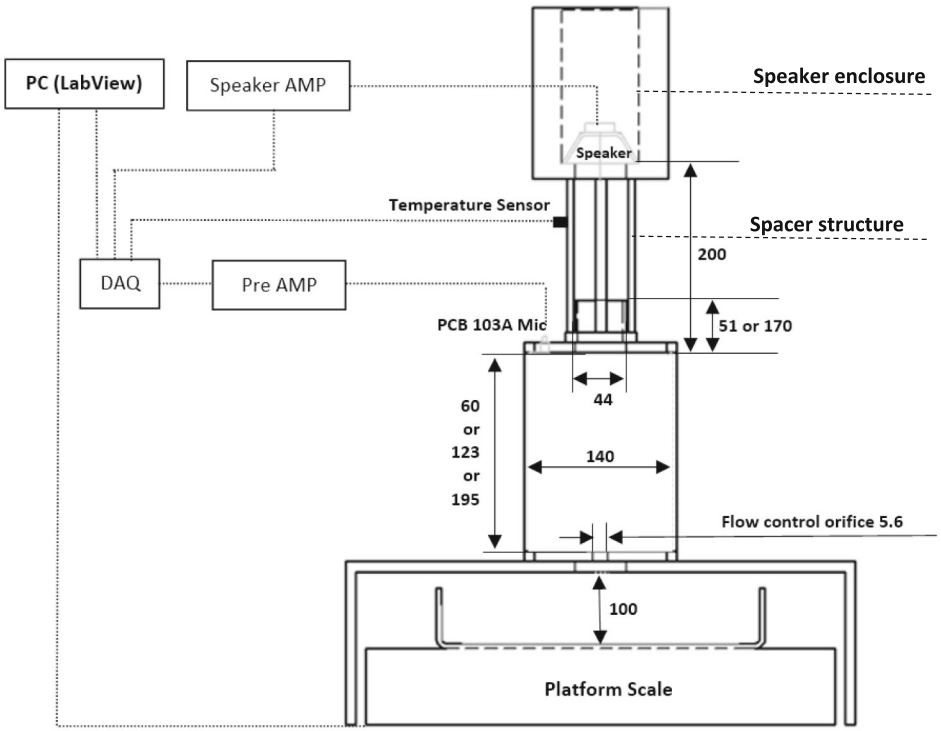

Fig. 6 Resonator apparatus for static and water discharge experiments. All dimensions are in mm

3.2 Variable Volume Resonator

A mechanically variable volume resonator initially designed and used in a study by Webster [36] was utilised for rapid volume measurement in a fast-changing cavity volume. Figure 7 shows the variable chamber apparatus. This apparatus consists of a cavity with a piston as the cavity floor, controlled by a stepper motor linear actuator (LXP B 200, SMC Corporation, USA) with the stepper motor controller SMC LC6D. The actuator was driven by pulses from the data-acquisition hardware, allowing a volume sweep of approximately 2100 mL with positional precision of ± 0.25 mL. The cavity of this device was made out of an aluminium tube with a wall thickness of 3 mm and an internal diameter of 156 mm. The port was 170 mm long with an internal diameter of 44 mm with 3 mm wall thickness. The microphone was inserted inside the cavity glued to the upper plate, 40 mm away from the port opening, with the microphone wire coming out of the resonator port, fixed to the port wall using tape. The excitation was by a subwoofer (TS-A300S4 12 inch Pioneer subwoofer, Pioneer, Japan) placed beside the resonator, 300 mm away from it, centre aligned.

4 Experimental Procedure

4.1 Determining Natural Frequency And Quality Factor

To obtain k_0, the resonator was continuously excited by a sweep through continuous chirp, and the microphone signal was simultaneously recorded. The sampling rate was 44,100 Hz, and the recording duration was 30 s. The recording underwent spectral analysis to obtain a power spectral density graph, and the power peak of the graph was taken as resonance frequency; ambient temperature was also recorded, for use in calculation of k_0. Quality factor (Q) was obtained using various methods through Eqns. (25), (26), and (30) for comparison. The estimated volumes in the results section are based on quality factor determined via the reference sample method (Eq. 26) because this approach provides direct Q determination from the same pressure-ratio measurements used in the SPQF model (Eq. 20), ensuring methodological consistency. Water filling approximately one-third of the cavity volume served as the reference sample, with volume measured gravimetrically to ± 2 mL.

4.2 Static Volume Measurement

The static volume measurements were conducted using the resonator apparatus depicted in Fig. 6. Various configurations were tested, including 1-L, 2-L, and 3-L cavities with 51-mm

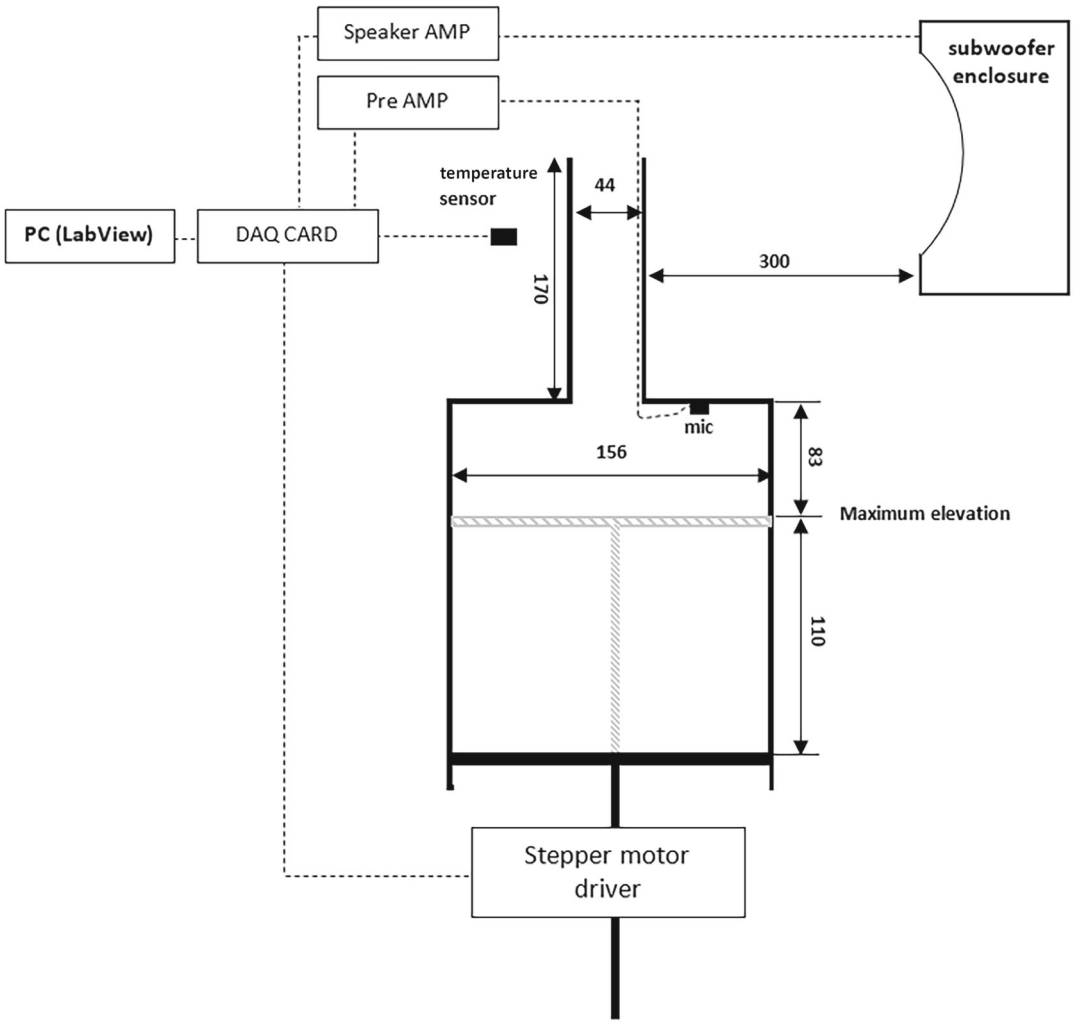

Fig. 7 Variable chamber apparatus. All dimensions are in mm

and 170-mm ports. The bottom of the resonator was sealed with a 12-mm-thick blank acrylic sheet. Resonator constants were determined using the methods outlined in Sect. 4.1. Initially, the resonator was excited at its natural frequency for 1 s. Half a second after the start of this excitation, the cavity pressure amplitude, denoted as P_0, was determined by the peak height of the pressure oscillation. This was recorded by the cavity microphone and averaged over 0.5 s. Samples were allowed to equilibrate with the laboratory environment for at least 2 h before measurement to ensure thermal equilibrium with the resonator. For water-fill tests, reverse-osmosis water was stored in the laboratory at ambient temperature prior to use. Subsequently, the resonator's cover plate was opened, and solid samples, specifically, glass spheres with diameters of 25 mm, 60 mm, and 80 mm, were introduced. After replacing the cover plate, the cavity pressure amplitude, P_1, was measured using the same method as for P_0 to obtain sound pressure ratio $\overline{P}$. The cavity content volume was calculated using the SPQF model (Sect. 2.2, Eq. 20).

4.3 Dynamic Volume Measurement of Discharging Water

The discharge orifice was blanked off using duct tape. A monotone equivalent to the natural frequency of the empty resonator was played on the speaker for 1 min, and at the one-minute mark, the sound pressure P_0 was sampled for 0.05 s. The delay was to allow temperature stabilization of the speaker coil for steady acoustic power output. Preliminary tests showed cavity pressure amplitude varied by 2–3% during the first few seconds of continuous operation before stabilising to < 0.1% variation after ~ 60 s, possibly due to voice coil heating affecting driver/amplifier response. In each test run, while the speaker was running, the resonator was filled with almost 2.5 kg of RO water. The duct tape

was removed to let the water discharge into the bucket on the platform scale. While the water sample was being discharged, sound pressure amplitude was tracked and sampled every 0.05 s to obtain $\overline{P}$ continuously. The water volume was then tracked using the SPQF model and compared with the resonator fill volume tracked by the mass of the discharged water.

4.4 Dynamic Cavity Volume Measurement Using The Mechanical Resonator

For the dynamic experiments conducted using the resonator shown in Fig. 7, the piston was positioned at maximum elevation and measurements were taken over 110 mm of travel (~ 2100 mL). The resonator's natural frequency was ascertained through excitation and spectral analysis, as detailed in Sect. 4.1. The value of P_0 was captured using the method given in Sect. 4.3. Subsequently, the piston was raised by 55 mm, and the sound pressure was documented to compute the quality factor using Eq. 26. Dynamic tests were initiated by allowing the piston to move 110 mm upward from its lowest position to its maximum elevation. This motion occurred while the system was excited at the resonator's natural frequency, set when the piston was fully lowered. Throughout the piston's travel, the sound pressure amplitude sampled in 20–40 ms windows by the internal resonator microphone was continuously monitored and recorded in alignment with the instantaneous piston position. This procedure was repeated at piston speeds ranging from 0.3 to 75 mm.s^{-1}.

5 Results

In this section, we report a capacity-normalised indicator, the relative error per cavity capacity as shown in Eq. 31 for cross-setup comparison. The metrological uncertainty as expanded uncertainty $U = ku_c$ with $k = 2$ (~ 95% coverage) where the combined standard uncertainty is the root-sum-square of Type A and Type B terms $u_c^2 = u_A^2 + u_B^2$. Type A (repeatability) is obtained from repeated sample volume determination using the SPQF method, and Type B (systematic) contributors include reference volume calibration, microphone sensitivity/linearity, temperature effects, resonator volume thermal expansion, Q calibration, DAQ timing/gain, and source stability.

$$E_{cap}\% = 100\left|\frac{V_A - V_S}{V_c}\right| \tag{31}$$

Using Eq. 20, first-order propagation gives the relative sensitivity of the reported volume to the main variables:

$$\frac{dV_s}{V_s} \approx \frac{dV_c}{V_c} - \frac{dQ}{Q} - \frac{1}{1-\bar{P}^2}\frac{d\bar{P}}{\bar{P}} \tag{32}$$

where V_c denotes cavity volume (± 0.83% from dimensional measurements), Q denotes quality factor (± 1.2% from reference volume and drive amplitude variation), and $1/(1-\overline{P}^2)$ denotes the fill-factor-dependent sensitivity term that amplifies pressure measurement uncertainty (± 1.0% base) to 1.3–2.0% depending on fill level. Temperature variation (± 2 °C) contributes ± 0.68% via speed of sound changes (Eq. 22). From Eq. 32:

$$\left(\frac{u_B}{V_s}\right)^2 \approx (\beta u_T)^2 + \left(\frac{u_Q}{Q}\right)^2 + \left(\frac{1}{1-\bar{P}^2}u_{\bar{P}}\right)^2 \tag{33}$$

where u_T, u_Q and $u_{\overline{P}}$ are the standard uncertainty terms.

Type B components evaluated from equipment specifications and measurement procedures:—Cavity volume: ± 0.83% (digital calipers ± 0.5 mm on D = 140 mm, H = 123 mm)—Temperature: ± 2 °C → ± 0.68% (LM35 sensor ± 0.5 °C plus spatial/temporal variations)—Quality factor: ± 1.2% (reference water ± 2 mL, drive amplitude variation Fig. 18)—Pressure ratio: ± 1.0% base (PCB 103A linearity ± 2% FS), amplified by $1/(1-\overline{P}^2)$ to 1.3—2.0% depending on fill factor Equipment: PCB 103A transducer (linearity ± 2% FS, 0.05—13 kHz), PCB 482A18 conditioner (SNR > 90 dB), LM35 temperature sensor (± 0.5 °C spec), verified against mercury thermometer (Brannan, 0.1 °C resolution, agreement ± 1 °C). Reference volumes: hydrostatic weighing (± 0.2 mL for 113—258 mL spheres), vernier callipers (marble diameters 15.97 ± 0.26 mm). Combined Type B: ~ 2.0% of measured volume. With Type A repeatability (0.5–0.7 mL typical, Table 1), expanded uncertainty (k = 2) is ~ 4% of measured volume, or ~ 0.2% when normalised by cavity capacity. Repeated measurements were consistently within the calculated total uncertainty, thereby demonstrating the systems measurement performance.

To compare the performance across different resonator sizes, we report capacity-normalised volume $E_{cap}\%$ (Eq. 31). Because the SPQF model scales V_s with V_c, normalising measurement error by V_c removes the first-order capacity scaling and enables cross-setup comparison.

It is noteworthy that $E_{cap}\%$ is not strictly size invariant. Sensitivity also depends on Q, $\overline{P}$, and operating conditions. Therefore, we present U (mL) alongside $E_{cap}\%$.

Table 1 Summary of representative static and dynamic volume determination experiments

Test / Material	Cavity & Port	Test type	Repeatability error u_A (k = 2) (mL)	MeanBias from parity (mL)	*Cavity capacity-normalised error (Bias ± Rep.)*	Notes
Marbles (Ø≈24.76 mm), incremental loading	3-L cavity, 51-mm port*;	Static (solids)	1.4	9.7	0.07% ± 0.05%	178 marbles from empty to near full; slight nonlinearity when nearly full up (> 80% cavity capacity)
Marbles (Ø≈24.76 mm), incremental loading	1-L cavity, 51-mm port*;	Static (solids)	1.7	0.2	0.02% ± 0.14%	Resonator capacity was 50 marbles; the results were linear up tp 42 marbles
Glass sphere Ø60 mm (V_A = 113.64 mL actual),	2-L cavity, 170-mm port*;	Static (solid)	0.4	0.3	0.01% ± 0.02%	Repeated 10 times. Negligible effect of sample position (centre vs side)
Glass sphere Ø80 mm (V_A = 258.10 mL actual)	2-L cavity, 170-mm port*	Static (solid)	0.6	0.5	0.07% ± 0.03%	
Marbles (Ø≈15.97 mm),	2-L cavity, 170-mm port*	Static (solids)	0.2	3.3	0.16% ± 0.01%	Aggregate load; within stated accuracy band confirmed by buoyancy measurement
Water discharge (free outflow) out of a 5.6 mm orifice	3-L cavity, 51-mm port*	Dynamic (liquid)	27.6	12.0	0.41% ± 0.96%	Occasional anomalies when water level > ~ 70% capacity;
Variable chamber, slow piston (0.3 mm·s^{-1}; ~ 5.7 mL·s^{-1})	Variable cavity ¬2 L displacement, 170-mm port*	Dynamic (mechanical volume sweep)	90	11.2	0.55% ± 0.55%	Measured at ~ 15 Hz; good tracking at low speed
Variable chamber, fast piston (75 mm·s^{-1}; ~ 1440 mL·s^{-1})	Variable cavity ~ 2 L displacement, 170 mm port*	Dynamic (mechanical volume sweep)	114.4	98.1	4.90% ± 4.90%	Deviation attributed to piston-induced noise & mean flow altering radiation damping/Q; full stroke in 1.436 s

*These numbers denote the physical port length (Refer to Sect. 1)

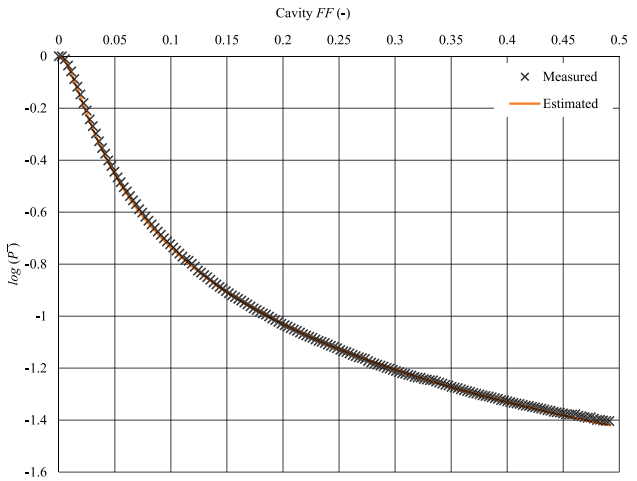

Fig. 8 Change in sound-pressure-amplitude ratio during sequential addition of 178 marbles (Ø 24.76 mm) to the 3-L resonator

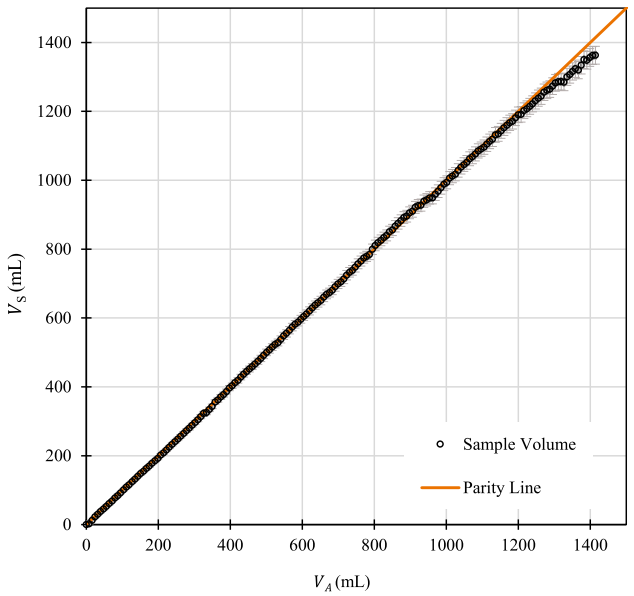

Fig. 9 Volume estimation of marbles (Ø 24.76 mm) when sequentially adding 178 of them to the 3-L resonator

The parameter fill factor, which indicates the portion of the cavity filled with the volume of the sample, V_B, is calculated using Eq. 34. Fill factor (FF) is obtained by dividing actual sample volume by resonator capacity.

$$FF = \frac{V_A}{V_c} \tag{34}$$

5.1 Static Volume Measurement

Figure 8, consistent with other experiments, displays the decrease in sound pressure amplitude when marbles with an average diameter of 24.76 mm and a solid volume of 7.95 mL ± 1.9% were introduced into the resonator. This resonator had a 3-L cavity and a port length of 51 mm. In this resonator setup, k_0 was 2.4857 m^{-1}, the reference value of Q was 53.47, and cavity volume was 2880 ± 2 mL. The marbles were added in increments of one marble at a time and the sound pressure inside the resonator was recorded before, and after, each addition. In total, 178 marbles were placed into the resonator. The estimated sound pressure $log(\overline{P})$ is calculated by rearranging Eq. 20 for pressure ratio in the form of Eq. 35, where V_A is the actual sample volume:

$$\overline{P} = \frac{V_c}{\sqrt{Q^2 V_A^2 + V_c^2}} \tag{35}$$

In this experiment, P_0 was 82.8 Pa (132 dB), which decreased to 3.2 Pa (104 dB) after loading the cavity with 178 marbles, essentially filling it to the top. (Decibel (dB) pressures were calculated with reference to 20 μPa.)

Figure 9 shows the estimated versus the actual volume V_A of the marble samples. The maximum error was 9.7 mL for up to $V_A = 1200$ mL (150 marbles). In this region, the mean absolute error (MAE) or bias from parity was 2.11 mL with an uncertainty of 0.72 mL.

Figure 10 shows the cavity-normalised measurement error of volume of marble samples, which are demonstrated in Fig. 9. For fill volumes higher than 1200 mL, where the resonator reaches ~ 85% of its capacity and higher, marbles interfere with the port opening, which results in a drop of accuracy and introduces nonlinearities in volume estimation.

Volume measurement on a bulk of marbles was repeated using the 1-L cavity with the resonance wavenumber k_0=4.5450 m^{-1}. The results of this experiment are shown in Fig. 11. For up to 42 marbles equivalent to $V_A = 330$ mL, the measurement uncertainty was 0.68 mL with a maximum error of 3.5 mL.

The experiment was repeated in the 2-L cavity and the 170-mm port; $k_0 = 1.9486$ m^{-1} and $Q = 37.89$. The results were similar to the experiments in the smaller cavity and the shorter port. This resonator was used to measure the volume of the large glass spheres. The glass spheres with almost 60 and 80 mm diameters had actual volumes of 113.6 and 258.1 mL, respectively. Reference volumes for large glass spheres were determined by hydrostatic weighing. (The expanded uncertainty k = 2 was ± 0.2 mL, accounting for balance precision and water density variation.) Each sample was placed in the centre of the resonator bottom plate. After measuring the sound pressure, the resonator was tilted to move the sample to the sides. The sound pressure ratio variation with sample position was negligible. The estimated volumes of the 60-mm and 80-mm spheres were 113.98 mL and 257.58 mL, respectively. The measurement error was 0.3 and − 0.5 mL. In another experiment, the same resonator was filled with ~

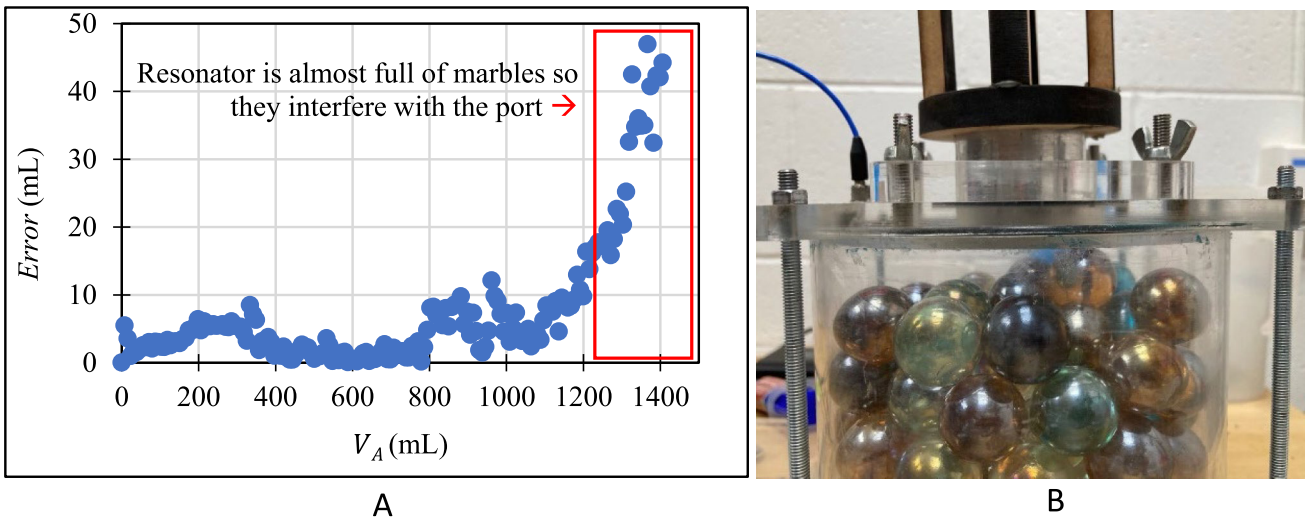

Fig. 10 Volume-estimate error versus actual added volume during sequential marble loading (A), with errors rising sharply when marbles begin to obstruct the port as the resonator nears full; photograph of port interference (B)

2 kg of small marbles with an average diameter of 15.97 ± 0.26 mm. The total solid volume of the marbles was 796.4 ± 8 mL where the uncertainty reflects diameter variation through N marbles. The SPQF estimate was 793.1 mL, within 0.5% of the calculated reference value.

5.2 Dynamic Liquid Volume Test

Figure 12 shows the estimated volume of water inside the cavity being freely discharged from the bottom of the cavity. Figure 13 shows the histogram of the capacity-normalised error E_{cap}% for the data presented in Fig. 12. The ordinate represents the normalised observation frequency (relative frequency) of the error values, illustrating the distribution and spread of measurement deviations around zero. Figure 14 compares the flowrate of 2.2 kg of water being discharged, estimated from the mass of discharged water and using the acoustic method.

In Fig. 14, the flowrate estimated from the mass recorded by the platform scales has a stepwise form. The reason is that the scale's precision was limited to ± 0.005 kg. The estimated flowrate using the acoustic method can be seen to follow the measurements taken by direct weighing.

5.3 Dynamic Tests on the Mechanically Variable Chamber

Figure 15 shows the experiment's results using the variable chamber resonator when the piston moved up at 0.3 mm.s^{-1} resulting in a cavity volume change at the 5.7 mL.s^{-1} rate. In Figs. 15 and 16, the ordinate is the estimated cavity volume as it changes with the piston position, and the abscissa is the actual cavity volume. On average, estimated volume had 11 mL of bias from the parity, with a standard deviation of 45 mL. The measurement rate in this experiment was ~ 15 Hz.

Figure 16 shows the experiment results when the piston moved up at 75 mm.s^{-1}, equivalent to 1440 mL.s^{-1} of volume displacement. The entire duration of the piston travel was 1.44 s. On average, the estimated volume had a bias of 98 mL from the parity. The contributors to this deviation are thought to include the noise induced by the piston and the air being pushed out of the port with a flow rate of 1440 mL.s^{-1}, which can affect the oscillating mass of the air in the port.

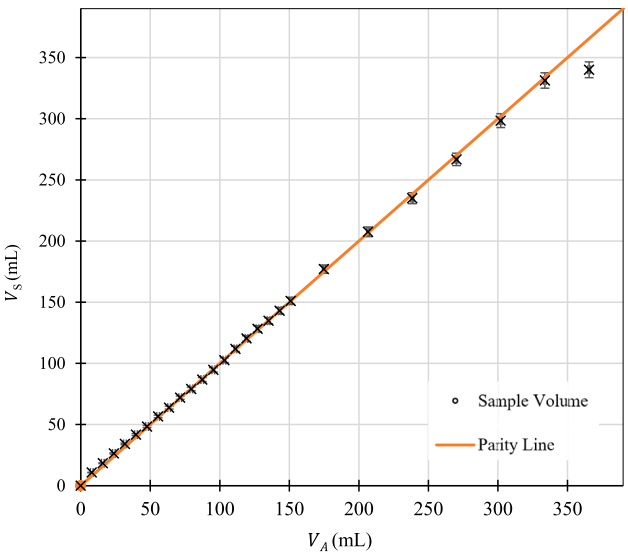

Fig. 11 Volume estimation of marbles in the 1-L resonator

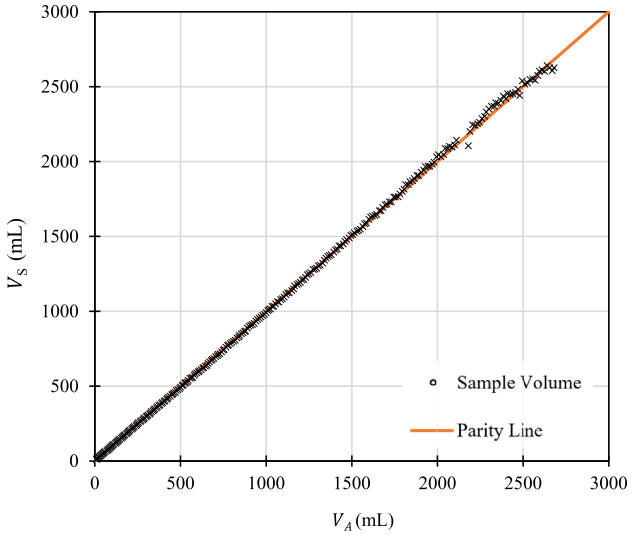

Fig. 12 Discharging water volume estimation

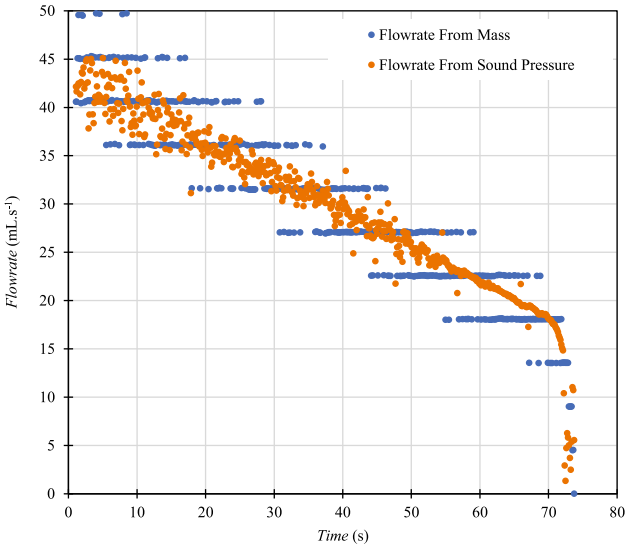

Fig. 14 Flowrate estimation of water out of the cavity from water mass and sound pressure tracking

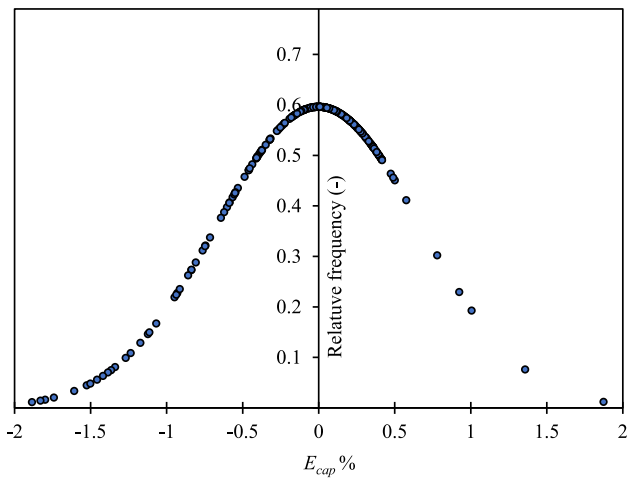

Fig. 13 Distribution of capacity-normalised error for the water-discharge volume estimation

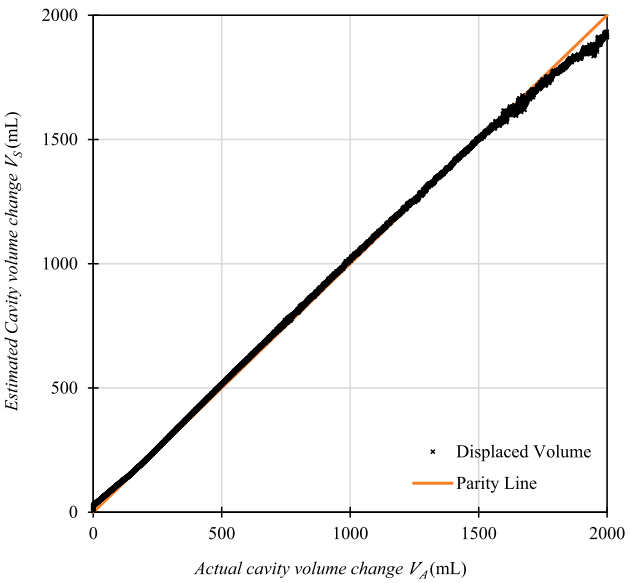

Fig. 15 Estimation of cavity volume change in the variable chamber resonator with a piston speed of 0.3 mm.s.$^{-1}$

6 Discussion

6.1 Model Verification

Filling the 3-L cavity (51-mm port) with solid marbles (Ø24.76 mm, incrementally loaded) resulted in a sound pressure ratio proportional to the occupied volume. The volume measurement results were highly linear up to a fill factor of 0.85–0.9, where a slight underestimation of the volume, with a repeatable pattern, was recorded. Interference of the sample inside the resonator with the oscillating mass of air in the port could contribute to this underestimation.

When exciting the resonators for obtaining sound pressure, there was a delay in the cavity pressure response rising to its stabilised level. The delay when using the 51-mm port was 0.2–0.3 s, while for the 170-mm port, it was nearly 0.5 s.

Consistent excitation of the resonator while the mass of water was being discharged made it possible to track the volume change inside the cavity through sound pressure ratio. Theoretically, the minimum time required for measuring sound pressure amplitude is one oscillation cycle. The sound pressure amplitude was measured for durations between 0.02 and 0.05 s, equivalent to 10–20 pressure oscillations to be averaged, and this time made it possible to track the flowrate of the liquid out of the cavity, confirmed by weighing.

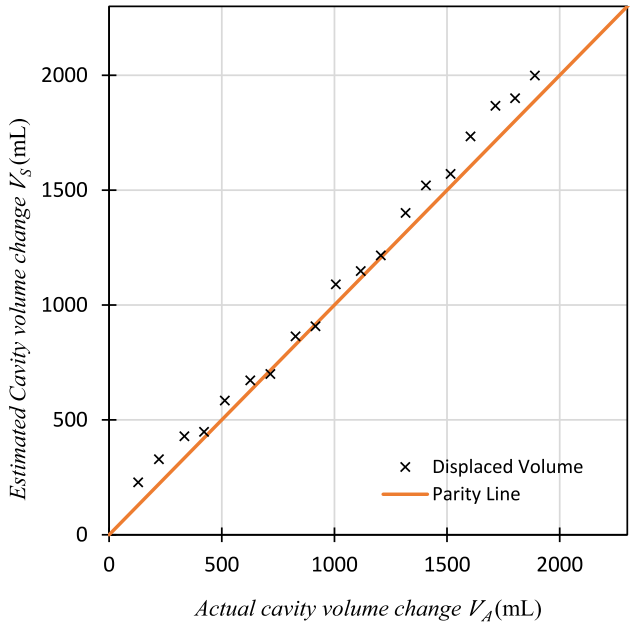

Fig. 16 Estimation of cavity volume change in the variable chamber resonator with a piston speed of 75 mm.s.$^{-1}$

One repeated observation in the water discharge test was when the water level was approximately two-thirds of the cavity height. An anomaly in pressure amplitude formed an outlier data point visible in Fig. 12 in $V_A = 2180$ mL with $E_{cap}\% = 3$. This could have been due to a secondary resonance or a resonance mode occurring within the port or speaker driver, manifesting as a cavity sound pressure surge for a certain point.

The mechanically variable chamber apparatus was used to assess the proposed model's capability to measure the volume of a cavity with a dynamic volume with a very high rate of change. The results presented in Fig. 16, typical for lower piston speeds, outline the proposed method's capability to track volume change in a highly dynamic situation.

It is noteworthy that in the development of the SPQF model, the resonator is assumed to have dimensions much smaller (< 10%) than the resonance wavelength. Accordingly, the present work should be regarded as a proof of concept. For other resonators such as asymmetric geometries or cavities/ports whose dimensions approach a significant fraction of the wavelength or are substantially narrow, general corrections for dimensional nonlinearities should be applied, as is standard in traditional Helmholtz resonance-based volume determination by frequency hunting.

The test materials used here were limited to solids and liquids in litre scale resonators. Porous materials, powders, and bulk solids are out of the scope of this study. This material may introduce additional nonlinearities and energy losses. Addressing such cases can be an important subject for future work.

Both the SPQF model and the Q-profile shifting (QPS) method of Webster [36] use a single-tone drive and monitor the resulting amplitude attenuation to determine sample volume; the present experiments also used apparatus designed by Webster. The methods differ in how amplitude is converted to volume. In QPS, the observed amplitude drop is mapped to a frequency shift via a pre-acquired resonance-peak profile, and the shifted frequency enters the Helmholtz equation (Eq. 1). This assumes that the profile shape is invariant with cavity fill; in practice it is not, the profile changes with fill level, so geometry-dependent second-order correction curves are required [36], Ch. 4), and the usable fill fraction is limited to ~ 15%. SPQF bypasses the frequency inference: Equation 20 relates $\overline{P}$ to V_s directly through the forced-vibration response, without assuming profile-shape invariance and without geometry-dependent corrections. The $1/(1-\overline{P}^2)$ term in Eq. 32 quantifies how pressure-ratio uncertainty is amplified with increasing fill; this divergence becomes significant only above fill factors of 0.85–0.9 (Figs. 9–10), extending the measurable range well beyond that of QPS.

Table 1 summarises the key experimental results of this section for quick reference. It is provided as an overview of the representative tests.

6.2 Accurate Assessment of the Quality Factor

Central to the SPQF model is the resonance quality factor Q. The experimental results suggest that a variation of 10% in Q can, on average, result in a 2% measurement error. Quality factors for the volume measurement rigs were assessed using undriven and driven methods, as discussed in Sect. 2.2. Figure 17, typical for the 51-mm port, shows the impulse (undriven) response of a 3-L resonator with a 170-mm port. The impulse was a 0.5-s chirp ranging from 84 to 86 Hz, while the resonance frequency was 85 Hz.

As shown in Fig. 17, the logarithm of pressure peaks has a linear trend ($R^2 = 0.999$) with $S = -5.06$. Using Eq. 30, the quality factor of this resonator is 51. This figure had a variation of 2% in repeated tests and did not show a significant variation with the strength of the applied impulse except for very low powers (< 1% of the speaker power) where the response was within the microphone's noise floor.

In contrast, when assessing the quality factor of the same resonator under driven oscillation, the quality factor showed a strong correlation with the driver amplitude. Figure 18 shows the quality factor estimated using driven oscillation (Ordinate) vs. the driver sound pressure (Abscissa) measured 10 mm above the resonator port. Relocating the speaker driver about the resonator port or adjusting the output power of the speaker affects the resonance quality factor. This observation was confirmed by testing various port lengths of 51,

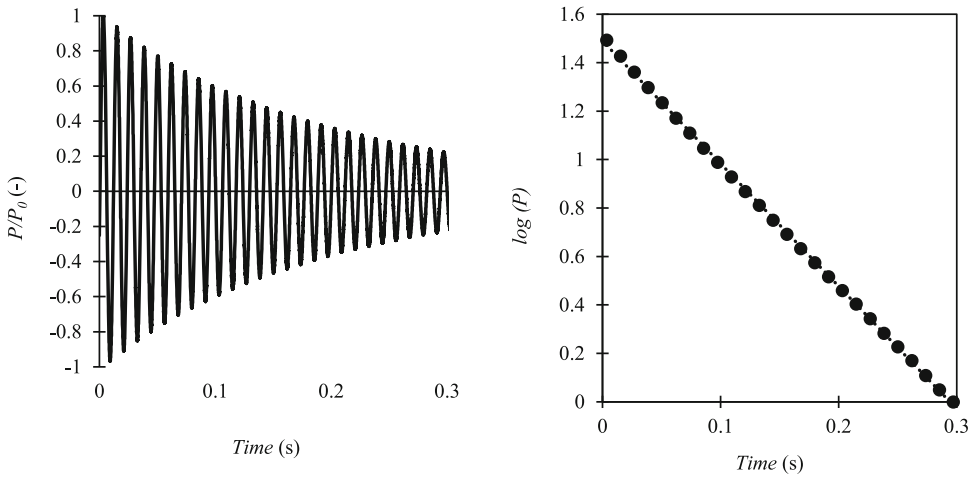

Fig. 17 Impulse response of the 3-L resonator

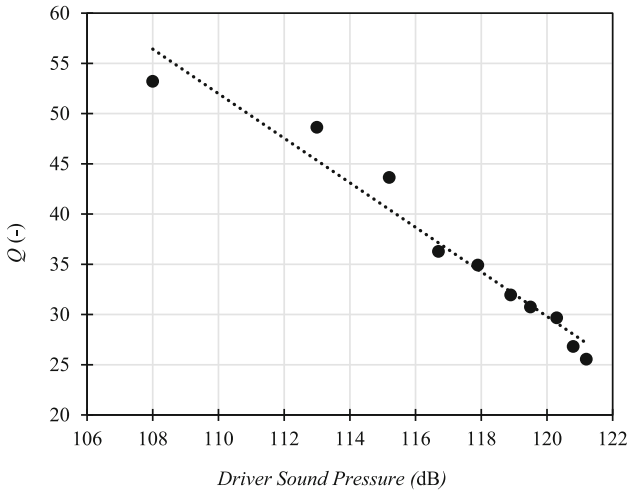

Fig. 18 Quality factor assessed in driven resonance

250, 500, and 1000 mm. In practice, outside anechoic conditions, nearby boundaries and objects can alter the incident pressure at the port. To minimise this, the constant-amplitude requirement should be defined in terms of local sound pressure level (SPL) at the port and not the amplifier voltage. In practice, the source, port assembly can be placed in a simple foam-lined, box enclosure or against a rigid baffle to suppress secondary reflections and standing wave problem, and a reference microphone at the port can be used to monitor SPL during acquisition. Because SPQF uses a single-frequency drive, slow drift in room gain mainly scales the response and is largely removed by baseline normalisation; still, keeping the local SPL stable improves repeatability.

The directly determined quality factors using a sample with known volume (Eq. 26) were within quality factors obtained by spectral analysis (Eq. 25) with an uncertainty of 10%.

The experimental observations suggest that when using the volume measurement method demonstrated in this paper, the most accurate results are obtained when the quality factor is calculated using Eq. 26.

7 Conclusion

We have developed and experimentally validated a model for accurately determining the volume of solid or liquid samples from the amplitude of cavity sound pressure. The method excites a ported cavity with a single-tone signal of constant amplitude at the natural frequency of the empty resonator. Introducing a sample reduces the effective cavity volume and, consequently, the steady-state sound-pressure amplitude. This amplitude change can be resolved over a window comparable to one period of the drive, enabling near-instantaneous volume estimation at rates on the order of tens of measurements per second, depending on the averaging window.

The hardware implementation comprises a Helmholtz-type resonator (cavity plus port), a commercially available loudspeaker and pressure microphone, a temperature sensor, and standard signal-generation and data-acquisition hardware. Three constants were required to calibrate the system—the empty-cavity volume, the resonator quality factor, and the natural-frequency wavenumber. These are obtained experimentally using the procedures detailed in this study. Once these constants are established for a given resonator, the setup can measure the volume of solid or liquid samples under both static and dynamic conditions.

We validated the method using water and various solid samples in 1-, 2-, and 3-L cavities. Across these static tests, the maximum error remained below 1% of cavity capacity, and for fill factors between 0.2 and 0.5 we achieved expanded uncertainties as low as 0.05–0.1% of capacity.

Dynamic tests were conducted using both water discharge and a mechanically variable-volume chamber. For

liquid discharge, the method successfully tracked cavity volume and derived flowrate, with capacity-normalised errors typically below 1%. In the mechanically driven chamber, the approach tracked volume changes at rates up to approximately 1440 $mL \cdot s^{-1}$, delivering instantaneous volume estimates with capacity-normalised errors of order a few percent in the most demanding cases.

This work therefore demonstrates a proof of concept for rapid, acoustics-based volume measurement using a single Helmholtz resonator and pressure-amplitude tracking. Practical deployment in applications such as in-line food processing, the study of foaming, or zero-gravity volume determination will require further engineering, including port and cavity design to minimise secondary resonances and standing waves, management of absorption in porous or highly attenuating media, and robust calibration of the quality factor under field conditions. Addressing these design aspects and extending the method to more complex materials and geometries are promising directions for future work.

Acknowledgements The first author gratefully acknowledges Massey University, New Zealand, for supporting this research through the Massey Doctoral Scholarship.

Funding Open Access funding enabled and organized by CAUL and its Member Institutions. This study was supported by the Massey University Doctoral Scholarship.

Declarations

Conflict of interest The authors declare that they have no conflict of interest.

References

1. Agnew, J.M., Leonard, J.J., Feddes, J., Feng, Y.: A modified air pycnometer for compost air volume and density determination. Can. Biosyst. Eng. **45**, 6–27 (2003)
2. Amorim, L.L., Mutz, F., De Souza, A.F., Badue, C., Oliveira-Santos, T., 2019. Simple and Effective Load Volume Estimation in Moving Trucks using LiDARs, in: 2019 32nd SIBGRAPI Conference on Graphics, Patterns and Images (SIBGRAPI). Presented at the 2019 32nd SIBGRAPI Conference on Graphics, Patterns and Images (SIBGRAPI), IEEE, Rio de Janeiro, Brazil, pp. 210–217. https://doi.org/10.1109/SIBGRAPI.2019.00036
3. Barzegar, M., Davies, C.E., Grafton, M.C.: Ultrasonic measurement of fill volume of bulk solids in discharge vessels. Powder Technol. (2024). https://doi.org/10.1016/j.powtec.2023.119339
4. Barzegar, M., Davies, C.E., Grafton, M.C., 2023. Rapid determination of the volume of granular material in a hopper using Helmholtz resonance, in: ICBMH2023: 14th International Conference on Bulk Materials Storage, Handling and Transportation: 14th International Conference on Bulk Materials Storage, Handling and Transportation. The Institution of Engineers, Australia Wollongong, NSW, pp. 74–81.
5. Barzegar, M., Redding, G.P., Davies, C.E., Fullard, L., Grafton, M.C.: Fill volume in a storage vessel determined by optical scanning. Powder Technol. (2024). https://doi.org/10.1016/j.powtec.2024.119532
6. Blackstock, D.T.: Fundamentals of physical acoustics. John Wiley & Sons (2000)
7. Blank, E.W., Willard, M.L.: Micro-density determination of solids and liquids. J. Chem. Educ. **10**, 109 (1933)
8. Bohn, D.A.: Environmental effects on the speed of sound. J. Audio Eng. Soc. **36**, 223–231 (1988)
9. Chanaud, R.C.: Effects of geometry on the resonance frequency of Helmholtz resonators. J. Sound Vib. **178**, 337–348 (1994). https://doi.org/10.1006/jsvi.1994.1490
10. Chen, H., Xu, H., Rao, X., Kondo, N., Bao, J., 2013. A Preliminary Study of Helmholtz Resonant for Measurement of Watermelon Volume, in: 2013 Kansas City, Missouri, July 21-July 24, 2013. American Society of Agricultural and Biological Engineers, p. 1.
11. Crosby, K.M., Williams, N.J., Werlink, R.J., Hurlbert, E.A.: Modal propellant gauging: High-resolution and non-invasive gauging of both settled and unsettled liquids in reduced gravity. Acta Astronaut. **159**, 499–507 (2019). https://doi.org/10.1016/j.actaastro.2019.01.050
12. García, A., Toral, V., Márquez, Á., García, A., Castillo, E., Parrilla, L., Morales, D.P.: Non-intrusive tank-filling sensor based on sound resonance. Electronics **7**, 378 (2018)
13. Indenbom, M.V., Pogossian, S.P.: Characteristics of partially filled Helmholtz resonators. Acta Acust. **7**, 51 (2023). https://doi.org/10.1051/aacus/2023039
14. Ingard, U.: On the theory and design of acoustic resonators. J. Acoust. Soc. Am. **25**, 1037–1061 (1953)
15. Inman, D.J.: Engineering Vibration. Prentice Hall (2001)
16. Kinsler, L.E., Frey, A.R., Coppens, A.B., Sanders, J.V.: Fundamentals of Acoustics. John Wiley & Sons. Inc, New York (2000)
17. Li, X., Li, Z., Zhang, R., Zhang, X., Chen, Y.: The effects of droplets and bubbles on on-orbit propellant volumetric measurements using cavity resonances. Microgravity Sci. Technol. **34**, 7 (2022). https://doi.org/10.1007/s12217-021-09924-1
18. Li, Z., Chen, Y., Li, X., Zhang, X., Chen, X.: Parameter analysis of on-orbit volumetric measurement using cavity resonance. Acta Astronaut. **166**, 113–122 (2020). https://doi.org/10.1016/j.actaastro.2019.10.003
19. Liang, H., Zhou, C., Li, S., Ma, X., Hendrich, N., Gerkmann, T., Sun, F., Stoffel, M., Zhang, J., 2020. Robust robotic pouring using audition and haptics, in: 2020 IEEE/RSJ International Conference on Intelligent Robots and Systems (IROS). IEEE, pp. 10880–10887.
20. Munjal, M.L.: Acoustics of ducts and mufflers with application to exhaust and ventilation system design. John Wiley & Sons (1987)
21. Nakano, A.: Study of liquid volume measurement for cryogens on orbit. TEION KOGAKU (Journal of Cryogenics and Superconductivity Society of Japan) **37**, 559–564 (2002)
22. Nakano, A., Nishizu, T.: Experimental study of liquid level gauge for liquid hydrogen using Helmholtz resonance technique. Cryogenics **77**, 43–48 (2016)
23. Nakano, A., Torikata, Y., Yamashita, T., Sakamoto, T., Futaya, Y., Nishizu, T.: Helmholtz resonance technique for measuring liquid

volumes under micro-gravity conditions. Microgravity Sci. Technol. **17**, 64–70 (2005). https://doi.org/10.1007/BF02872089
24. Nakano, A., Torikata, Y., Yamashita, T., Sakamoto, T., Futaya, Y., Tateno, A., Nishizu, T.: Liquid volume measurement with a closed Helmholtz resonator under micro-gravity conditions. Cryogenics **46**, 126–131 (2006)
25. Nishizu, T., Ikeda, Y., Manmoto, S., Umehara, T., Mizukami, T., 2001. Automatic, continuous food volume measurement with a Helmholtz resonator. Agricultural Engineering International: CIGR Journal.
26. Njane, S.N., Shinohara, Y., Kondo, N., Ogawa, Y., Suzuki, T., Nishizu, T.: Improved underwater Helmholtz resonator with an open cavity for sample volume estimation. Comput. Electron. Agric. **147**, 18–26 (2018). https://doi.org/10.1016/j.compag.2018.02.015
27. Panton, R.L., Miller, J.M.: Resonant frequencies of cylindrical Helmholtz resonators. J. Acoust. Soc. Am. **57**, 1533–1535 (1975)
28. Pozzebon, A., Benini, M., Bocci, C., Fort, A., Parrino, S., Rapallo, F.: Grid-layout ultrasonic LoRaWAN-based sensor networks for the measurement of the volume of granular materials. Measurement **220**, 113404 (2023). https://doi.org/10.1016/j.measurement.2023.113404
29. Rao, S.S., 2017. Mechanical Vibrations. Pearson Education, Incorporated.
30. Rayleigh, J.W.S.: The Theory of Sound, vol. vol. I and II. Dover Publications, New York (1945)
31. Rienstra, S.W., Hirschberg, A., 2004. An introduction to acoustics.
32. Selamet, A., Dickey, N.S., Radavich, P.M., Novak, J.M.: Theoretical, computational and experimental investigation of Helmholtz resonators: one-dimensional versus multi-dimensional approach. SAE Tech. Pap. Ser. (1994). https://doi.org/10.4271/940612
33. Tang, P.K., Sirignano, W.A.: Theory of a generalized Helmholtz resonator. J. Sound Vib. **26**, 247–262 (1973)
34. Thudium, J.: A gas pycnometer (microliter) for determining the mean density of atmospheric aerosol particles. J. Aerosol Sci. **7**, 167–173 (1976)
35. Vandegrift, G.: Experimental study of the Helmholtz resonance of a violin. Am. J. Phys. **61**, 415–421 (1993)
36. Webster, E.S., 2010. The application of Helmholtz resonance to determination of the volume of solids, liquids and particulate matter: a thesis presented in partial fulfilment of the requirements for the degree of Doctor of Philosophy in Instrumentation and Process Engineering (PhD Thesis). Massey University.
37. Webster, E.S., Davies, C.E.: The use of Helmholtz resonance for measuring the volume of liquids and solids. Sensors **10**, 10663–10672 (2010)
38. Wilson, J., Sterling, A., Lin, M.C., 2019. Analyzing liquid pouring sequences via audio-visual neural networks, in: 2019 IEEE/RSJ International Conference on Intelligent Robots and Systems (IROS). IEEE, pp. 7702–7709.